Effect of Hydrostatic Pressure and Temperature on the Performance of a One-Dimensional Photonic Crystal-Based Biosensor

Samad Roshan Entezar

Department of Physics, University of Tabriz, Tabriz, Iran

Corresponding author email: s-roshan@tabrizu.ac.ir

Regular paper: Received: Sep. 5, 2021, Revised: Feb. 7, 2022, Accepted: Feb. 9, 2022, Available Online: Feb. 30, 2022, DOI: 10.52547/ijop.15.2.179

ABSTRACT—We theoretically analyze the sensing properties of a one-dimensional photonic crystal-based biosensor for detecting cancer cells infiltrated in a defect cavity layer. The biosensor consists of a sample cavity layer sandwiched between two identical photonic crystals of $Hgba_2Ca_2Cu_3O_{8+\delta}$ and GaAs. We use the transfer matrix method to evaluate the performance of the biosensor. We show that a defect mode appears in the transmission spectrum of the biosensor that its position depends on the type of cancer cells in the cavity layer. The analysis is carried out by comparing the transmittance peaks of the cancer cells with the normal cells. We investigate the performance of the biosensor under different hydrostatic pressures and temperatures. We show that one can use temperature change to fine-tune the frequency of the defect modes. In addition, we can adjust the working area of the biosensor by changing the hydrostatic pressure. It is shown that the sensitivity of the biosensor is independent of the temperature, while it strongly depends on the hydrostatic pressure.

KEYWORDS: biosensor, defect mode, hydrostatic pressure, photonic crystal, semiconductor, superconductor, temperature.

I. INTRODUCTION

Photonic crystal (PC) can be used as excellent optical sensors to detect multi-physical parameters such as concentration, temperature, pressure, etc. [1]-[5]. PCs are structures with a spatial periodic refractive index that are formed using alternating layers of material [6], [7]. The spatial periodicity of PCs prevents the propagation of light at certain frequency intervals known as photon band gaps (PBGs) [8]. The optical properties of photonic crystals mainly depend on the refractive index and thickness of the constituent materials [9]. By breaking the periodicity of the PC and creating a defect layer in them, some part of the light, known as a resonance peak or defect mode, may propagate through the PBG region [10]. The most important advantage of using defect modes is their very high sensitivity to small changes in the refractive index of the defect layer. Relying on this feature of defect modes and the uniqueness of their position encourage us to benefit the PC-based biosensors to differentiate different analytes [11]. The PC-based biosensors are compact, have a wide dynamic range, and are capable of real-time monitoring. The use of one-dimensional (1D) PCs in the construction of sensors has attracted considerable attention because they are easy to manufacture and have fewer parameters to optimize [12], [13].

The detection of cancer as the second leading cause of death worldwide is a challenging task in the medical field. Cancer, which kills tens of millions of people each year, is caused by different factors such as the lack of physical activity, tobacco, poor diet, and exposure to chemicals, radiation, or microbiological objects [14]. The refractive index of cancer cells compared to healthy cells is significantly increased due to the high amount of protein [15], [16]. This key feature can be used in the

early detection of cancer cells by optical biosensors. PC-based biosensors operate by measuring the wavelength change of the defect mode by variation of the analyte's refractive index.

In this study, we design a 1D-PC-based biosensor to monitor the various cancer cells. The healthy cells and the cancer cells placed in between two identical 1D-PCs composed of superconducting and semiconducting materials act as a defect and result in wavelength shifts of the defect modes appearing in the transmission spectra of the PBG. A change in the cancer cells causes a substantial change in the defect mode's ferequency. Thus, it is possible to identify different cancer cells by observing the transmission spectra of the 1D-PC-based biosensor. We use the transfer matrix method (TMM) to obtain the transmission spectra of the structure. Superconducting materials have fewer losses compared to the losses observed in PCs made of metals [17]. The dielectric constant of superconducting materials depends on the hydrostatic pressure and temperature because the superconducting materials' critical temperature varies with the hydrostatic pressure. In addition, the thickness and dielectric constant of the other 1D-PC layer, which is a GaAs semiconductor, also depend on the hydrostatic pressure. The dielectric constants of semiconductors are among its most important properties. Their magnitudes and temperature dependences are important for both fundamental and applied considerations. These properties enter in an important way into the physics underlying the optical properties of semiconductors. It is thus necessary to understand their dielectric properties and temperature. Toward this end the effects of temperature and hydrostatic pressure on the low-frequency dielectric constants of several crystals representative of III-V compounds (GaAs and GaP), II-VI compounds (ZnS and CdS), and group-IV (Si) semiconductors have been investigated in reference [18]. In this paper, we modify parameters such as hydrostatic pressure, temperature, and defect layer thickness and measure their effects on the sensitivity of the biosensor. This paper is organized as follows. Section 2 introduces the theoretical model with the main equations used. Section 3 discusses the numerical results for the transmission spectrum of the structure. Finally, the conclusions are summarized in Section 4.

II. Model and Basic Equations

Figure 1 schematically shows our considered 1D-PC-based biosensor composed of an analyte defect layer D with thickness d_D and refractive index, n_D embedded between two 1D-PC. The 1D-PCs with the structure (AB)" are constructed from n periods of the superconducting layer A and semiconducting layer B stacked along the z-axis direction. Here, we show the thicknesses of layers A and B with d_A and d_B and their refractive indices of n_a and n_b.

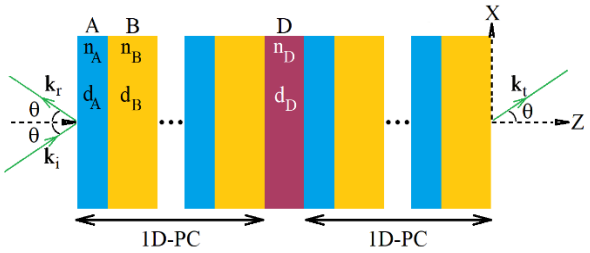

Fig. 1. Schematic representation of the 1D-PC-based biosensor with the structure $(AB)^5D(AB)^5$.

Figure 1 represents a plane wave with the temporal part $\exp(i\omega t)$ be injected from air into the biosensor at the incident angle θ. We use the transfer matrix method to calculate the transmittance of the structure. According to the transfer matrix method the total transfer matrix of the structure is given as:

$$M = (M_A M_B)^n M_D (M_A M_B)^n . \quad (1)$$

here,

$$M_j = \begin{pmatrix} \cos k_{jz} d_j & -\frac{i}{\alpha_j}\sin k_{jz} d_j \\ -i\alpha_j \sin k_{jz} d_j & \cos k_{jz} d_j \end{pmatrix}, \quad (2)$$

where, $j = A, B, D$, $k_{jz} = \frac{\omega}{c}\sqrt{n_j^2 - \sin^2\theta}$ is the z component of the wave vector, and

$$\alpha_j = \begin{cases} -\dfrac{k_{jz}}{\omega\mu_0} & for \quad \text{TE polarization} \\ \dfrac{k_{jz}}{\omega\varepsilon_0\varepsilon_j} & for \quad \text{TM polarization} \end{cases}. \tag{3}$$

Using Eq. (1) the transmittance of the structure are determined as:

$$T = \left| \frac{2}{M_{11} + M_{220} + M_{12}\alpha_0 + M_{21}/\alpha_0} \right|^2. \tag{4}$$

Here,

$$\alpha_0 = \begin{cases} -\dfrac{\cos\theta}{\eta_0} & for \quad \text{TE polarization} \\ \eta_0 \cos\theta & for \quad \text{TM polarization} \end{cases}, \tag{5}$$

and η_0 is the impedance of vacuum.

III. Results and Discussion

We choose $HgBa_2Ca_2Cu_3O_{8+\delta}$ as the superconducting material and GaAs as the semiconducting material, respectively, in our suggested model system. To describe the electromagnetic response of the superconductor layers in the absence of an external magnetic field, we adapt the Gorter-Casimir two-fluid model [19]. The complex dielectric constant of the $HgBa_2Ca_2Cu_3O_{8+\delta}$ superconductor is given by [20], [21]:

$$\varepsilon_A(\omega) = 1 - \frac{\omega_p^2}{\omega^2}, \tag{6}$$

where, $\omega_p = c/\lambda_L$ is the plasma frequency, c is the speed of light, $\lambda_L = \lambda_0 \Big/ \left(1-(T/T_C)^3\right)^{1/3}$ is the temperature-dependent London penetration depth, $\lambda_0 = 6.1\mu m$ is the London penetration depth at $T = 0\,K$, and $T_C = a_1 + a_2 P + a_3 P^2$ is the hydrostatic pressure-dependent critical temperature. Here, P is the hydrostatic pressure, $a_1 = 134\,K$, $a_2 = 2.009 \quad K/GPa$, and $\alpha_3 = -0.04194\ K/(GPa)^2$. The dielectric constant of the GaAs semiconducting layers B is given as [22]:

$$\varepsilon_B(\omega) = \left(\varepsilon' + Ce^{T/T_0}\right)e^{-\alpha P}, \tag{7}$$

which it depends on both the hydrostatic pressure and the temperature. Here, $\varepsilon' = 12.446$, $C = 21.125$, $\alpha = 0.0173\,GPa$, $T_0 = 240.7\,K$. Moreover, the thickness of the semiconducting layers B decreases by increasing hydrostatic pressure P as:

$$d_B = d_{0B}(1 - SP), \tag{8}$$

where d_{0B} is the thickness of layers B at P=0 and $S = 0.0042\ GPa^{-1}$ [23]. The defect layer L, which acts as a container, is filled with normal, Jurkat, HeLa, PC12, MDA-MB-231, and MCF-7 analyte cancer cells. The dielectric constants of the cells used in the calculations are listed in Table 1.

Table **1** The dielectric constants of the defect layer $_D$.

Analyte type	Dielectric constant
Normal cell	1.8225
Jurkat	1.932100
HeLa	1.937660
PC12	1.946025
MDA-MB-231	1.957201
MCF-7	1.962801

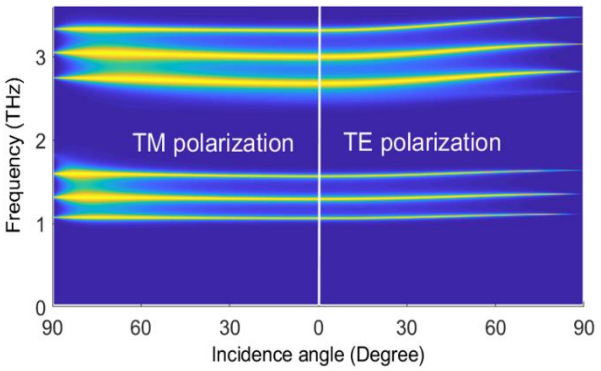

Fig. 2. The transmittance of the 1D-PC with the structure $(AB)^5$ in the plane (f,θ). Here, d_A=5 μm, d_{0B}=20 μm, T=4.2 K, and P=1 atm.

We begin our investigation by plotting the transmittance of the 1D-PC with the structure $(AB)^5$ in the plane (f,θ) in Fig. 2. Here, we assume d_A=5 μm, d_{0B}=20 μm, T=4.2 K, and P=1 atm. The transmittance of this 1D-PC shows an omnidirectional PBG at the frequencies less than 1 THz. Now, we limit our attention to this frequency range and plot the

transmittance of the 1D-PC-based biosensor with the structure $(AB)^5D(AB)^5$ versus frequency f for a) the TE-polarized and b) the TM-polarized incident waves at three different incidence angles θ in Fig. 3. Here, we assumed that the defect layer D with the thickness $d_D = 20\ \mu m$ is filled with the normal cells, and the other parameters are same as Fig. 2. Figure 3 reveals that the defect mode of the 1D-PC-based biosensor filled with the normal cells experiences a blue shift to higher frequencies by increasing the angle of incidence of light.

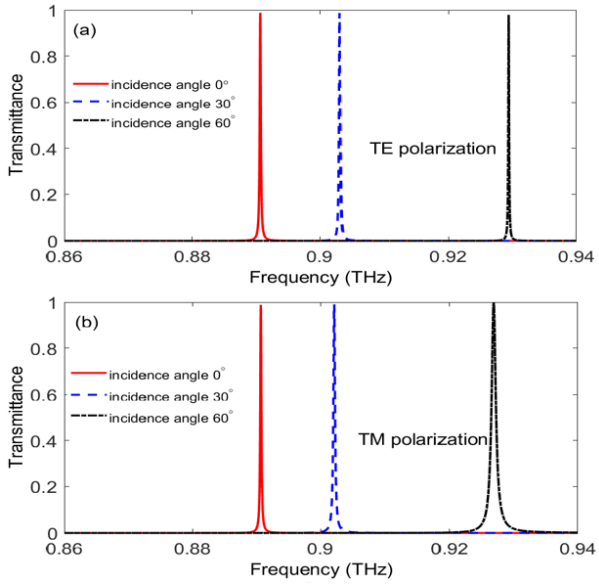

Fig. 3. The transmittance of the 1D-PC-based biosensor with the structure $(AB)^5D(AB)^5$ versus the frequency f for a) the TE-polarized and b) the TM-polarized incident waves at three different incidence angles θ. Here, we assumed that the defect layer D with the thickness d_D=20 μm is filled with the normal cells, and the other parameters are the same as in Fig. 2.

In addition, the location of the defect modes has a slight dependence on the polarization type of the incident light. The Q-factor $(Q = f_{Peak}/\Delta f_{FWHM})$ is an essential parameter to determine the performance of any sensor. Here, f_{Peak} is the peak frequency of the defect mode, and Δf_{FWHM} is the full width at half maximum frequency. The Q-factor of our biosensor has a considerably high value ~ 4400.

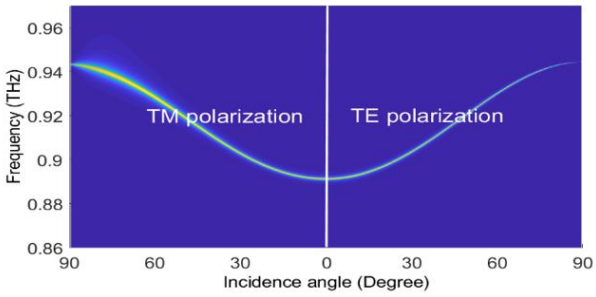

Fig. 4. The transmittance of the 1D-PC-based sensor with the structure $(AB)^5D(AB)^5$ in the plane (f,θ). The parameters used here are the same as in Fig. 3.

In Fig. 4 we illustrate the transmittance of the 1D-PC-based biosensor with the structure $(AB)^5D(AB)^5$ in the plane (f,θ). The figure shows that the width of the TM-polarized defect modes (Δf_{FWHM}) is greater than the TE-polarized ones. In addition, the width of the TM-polarized defect modes increases with increasing incidence angle, which leads to a reduction in the Q-factor of these defect modes. Hence, in what follows, we limit our investigations to the incidence angle $\theta = 0$.

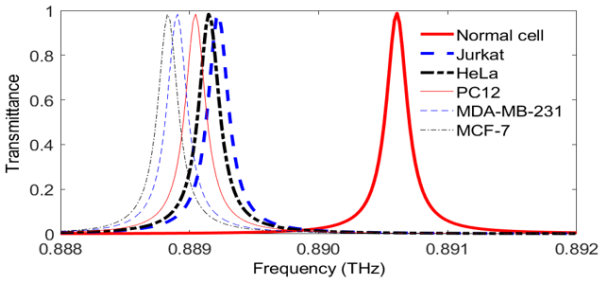

Fig. 5. The transmittance of the 1D-PC-based biosensor with the structure $(AB)^5D(AB)^5$ versus the frequency f at the incidence angle $\theta = 0$ for various analyte types (normal cells (the thick solid line), Jurkat (the thick dashed line), HeLa (the thick dash-dot line), PC12 (the thin solid line), MDA-MB-231 (the thin dashed line), MCF-7 (the thin dash-dot line). The other parameters used here are the same as in Fig. 3.

Now, we plot the transmittance of the 1D-PC-based biosensor with the structure $(AB)^5D(AB)^5$ versus the frequency f for various analyte types at the normal incidence in Fig. 5. Here, we see that the defect modes attributed to the cancer cells shift to the lower frequencies by changing the analyte type and increasing the refractive index of cancer cells.

The difference between the defect modes' frequencies attributed to the normal cells and cancer cells $\left(\Delta f = f_{normal\ cells} - f_{cancer\ cells}\right)$ to the corresponding difference between their refractive indices $\left(\Delta n = n_{normal\ cells} - n_{cancer\ cells}\right)$ is known as sensitivity $\left(S = |\Delta f / \Delta n|\right)$. The sensitivity ($S$) of our considered 1D-PC-based biosensor for different types of cancer cells is summarized in Fig. 6. Here, the detection sensitivity, which is about $\sim 13 GHz/RIU$, describes the potential of the proposed 1D-PC-based biosensor while varying the refractive index of cancer cells from 1.9321 to 1.9628.

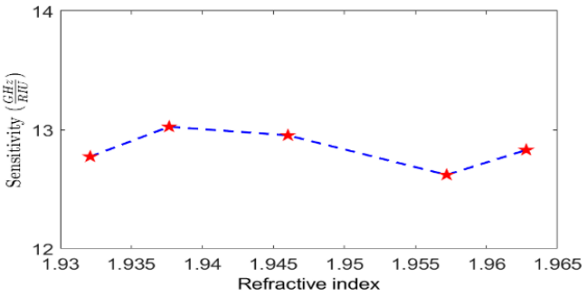

Fig. 6. The sensitivity (S) of the 1D-PC-based biosensor with the structure $(AB)^5D(AB)^5$ versus the refractive index, n, of the analyte cancer cells. The parameters used here are the same as in Fig. 3.

To continue, we want to investigate the effect of different parameters such as temperature, pressure, and thickness of the defect layer on the frequency of defect modes and the sensitivity of the biosensor. In Fig. 7, we plotted the peak frequency of the defect modes of the system versus the refractive index, n, of the analyte cancer cells at different temperatures. The figure reveals that the peak frequency of the defect modes slightly depends on the temperature and is red shifted by increasing the temperature. On the other hand, the difference between the defect modes' peak frequencies of the normal cells and the cancer cells does not depend significantly on temperature. Therefore, the sensitivity of the system is independent of temperature.

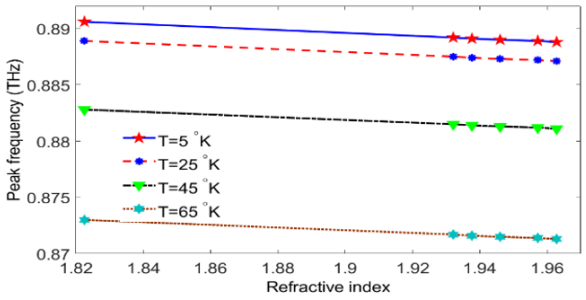

Fig. 7. The peak frequency of the defect modes of the 1D-PC-based biosensor with the structure $(AB)^5D(AB)^5$ versus the refractive index n, of the analyte cancer cells at different temperature T. The other parameters used here are the same as in Fig. 3.

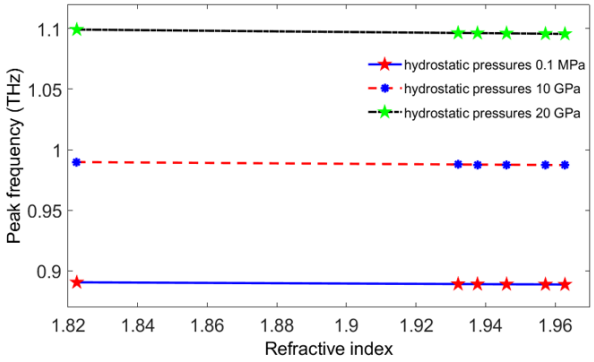

Fig. 8. The peak frequency of the defect modes of the 1D-PC-based biosensor with the structure $(AB)^5D(AB)^5$ versus the refractive index, n, of the analyte cancer cells at different hydrostatic pressures P. The other parameters used here are the same as in Fig. 3.

Figure 8 illustrates the peak frequency of the defect mode of the 1D-PC-based biosensor versus the refractive index, n, of the analyte cancer cells at different hydrostatic pressures. Here, the peak frequency of the defect modes strongly depends on the hydrostatic pressure and is blue shifted by increasing the hydrostatic pressure. Therefore, we can effectively adjust the biosensor detection area by changing the hydrostatic pressure. The effect of the hydrostatic pressure on the sensitivity of the biosensor is also shown in Fig. 9. Here, the detection sensitivity increases from $\sim 13 GHz/RIU$ to $\sim 25 GHz/RIU$ by rising the hydrostatic pressure from the $\sim 0.1 MPa$ to $\sim 20 GPa$. Therefore, from a diagnostic point of view, using the biosensor at higher pressures is preferable.

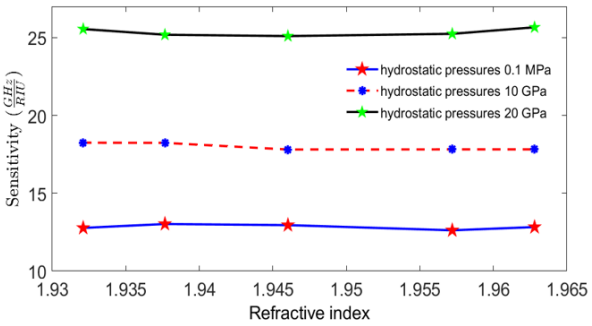

Fig. 9. The sensitivity (S) of the 1D-PC-based biosensor with the structure $(AB)^5D(AB)^5$ versus the refractive index, n, of the analyte cancer cells at different hydrostatic pressures P. The other parameters used here are the same as in Fig. 3.

In Fig. 10 we plotted the peak frequency of the defect modes of the 1D-PC-based biosensor versus the refractive index, n, of the analyte cancer cells for different thicknesses of the analyte defect layer. Here, the peak frequency of the defect mode moves to the lower frequency by increasing the thicknesses of the analyte defect layer. Figure 11 shows the sensitivity of the 1D-PC-based biosensor versus the refractive index, n, of the analyte cancer cells for different thicknesses of the analyte defect layer. Here, an increase of the analyte defect layer thickness from $20\,\mu m$ to $40\,\mu m$ increases the sensitivity from $\sim 13 GHz/RIU$ to $\sim 29 GHz/RIU$.

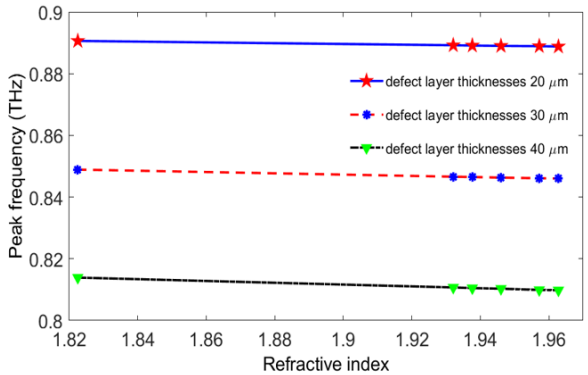

Fig. 10. The peak frequency of the defect modes of the 1D-PC-based biosensor with the structure $(AB)^5D(AB)^5$ versus the refractive index, n, of the analyte cancer cells for different thicknesses of the defect layer. The other parameters used here are the same as in Fig. 3.

From an experimental point of view, the temperature and pressure of our considered biosensor sensor can be controlled and adjusted by a cryogenic cooling system. Then we can measure the transmission spectrum of the system in the desired frequency range using a suitable light source and detector.

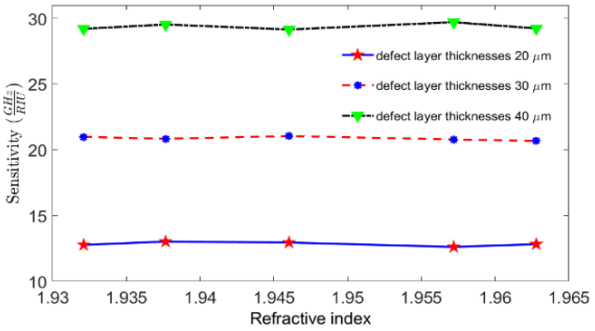

Fig. 11. The sensitivity (S) of the 1D-PC-based biosensor with the structure $(AB)^5D(AB)^5$ versus the refractive index, n, of the analyte cancer cells for different thicknesses of the defect layer. The other parameters used here are the same as in Fig. 3.

IV. CONCLUSION

We theoretically proposed a biosensor based on a defective 1D-PC composed of alternating superconductor and semiconductor layers. We calculated the transmittance spectrum using the transfer matrix method by changing the temperature, hydrostatic pressure, and defect layer thickness. We found that increasing the temperature and the defect layer thickness causes the resonance modes to move toward lower frequencies. On the other hand, the defect modes move toward higher frequencies by increasing the hydrostatic pressure. We also found that the sensitivity of the purposed biosensor is independent of the temperature and increases by increasing the hydrostatic pressure and defect layer thickness. The indicated sensitivity describes the potential of the proposed 1D-PC-based biosensor for the detection of various cancer cells.

REFERENCES

[1] Y. Chang, Y. Jhu, and C. Wu, "Temperature dependence of defect mode in a defective photonic crystal," Opt. Commun. Vol. 285, pp. 1501–1504, 2012.

[2] Y. Liu and H.W.M. Salemink, "All-optical on-chip sensor for high refractive index sensing in photonic crystals," Europhys. Lett. Vol. 107 pp. 34008 (1-5) , 2014.

[3] S. Zheng, B. Shan, M. Ghandehari, and J. Ou, "Sensitivity characterization of cladding modes in long-period gratings photonic crystal fiber for structural health monitoring," Measurement, Vol. 72, pp. 43–51, 2015.

[4] Y. Zhang, Y. Zhao, and Q. Wang, "Measurement of methane concentration with cryptophane E infiltrated photonic crystal microcavity," Sens. Actuators B: Chem. Vol. 209, pp. 431–437, 2015.

[5] Singh, K.B. Thapa, and N. Kumar, "Analysis and design of optical biosensors using one-dimensional photonic crystals," Optik, Vol. 126, pp. 244–250, 2015.

[6] J.D. Joannopoulos, P.R. Villeneuve, and S. Fan, "Photonic crystals: putting a new twist on light," Nature, Vol. 386, pp. 143–149, 1997.

[7] E. Yablanovitch, "Photonic crystals: semiconductors of light," Sci. Am. Vol. 285, pp. 46–55, 2001.

[8] J.C. Knight, J. Broeng, T. Birks, and P. Russell, "Photonic band gap guidance in optical fibers," Science, Vol. 282, pp. 1476–1478, 1998.

[9] B. Suthar and A. Bhargava, "Temperature-dependent tunable photonic channel filter," IEEE Photon. Technol. Lett. Vol. 24, pp. 338–340, 2012.

[10] P. Lalanne, C. Sauvan, and J.P. Hugonin, "Photon confinement in photonic crystal nanocavities," Laser Photonics Rev. Vol. 2, pp. 514–526, 2008.

[11] A.B. Suthar and A. Bhargava, "Biosensor Application of One-Dimensional Photonic Crystal for Malaria Diagnosis," Plasmonics, Vol. 16, pp. 59–63, 2021.

[12] J. Li, T. Tang, Y. Zhang, L. Luo, and P. Sun, "Magneto-plasmonic sensor with one dimensional photonic crystal for methane detection," Optik, Vol. 155, pp.74–80, 2018.

[13] A. Soltani, F. Ouerghi, F. AbdelMalek, and S. Haxha, "Comparative study of one-dimensional photonic crystal heterostructure doped with a high and low-transition temperature superconducting for a low-temperature sensor," Opt. Commun. Vol. 445, pp. 268–272, 2019.

[14] A.M. Soto and C. Sonnenschein, "Environmental causes of cancer: endocrine disruptors as carcinogens," Nat. Rev. Endocrinol, Vol. 6, pp. 363–370, 2010.

[15] C. Alibert, B. Goud, and J.B. Manneville, "Are cancer cells really softer than normal cells?," Biol. Cell, Vol. 109, pp. 167–189, 2017.

[16] M.A. Jabin, K. Ahmed, M.J. Rana, B.K. Paul, M.M. Islam, D. Vigneswaran, and M.S. Uddin, "Surface plasmon resonance based titanium coated biosensor for cancer cell detection," IEEE Photon. J. Vol. 11, pp. 1–10, 2019.

[17] L. Gonzalez, J. Ordonez, G. Zambrano, and N. Porras-Montenegro, "$YBa_2Cu_3O_{7-x}/BaTiO_3$ 1D superconducting photonic crystal with tunable broadband response in the visible range," J. Supercond. Novel Mag. Vol, 31, pp. 2003–2009, 2018.

[18] G.A. Samara, "Temperature and pressure dependences of the dielectric constants of semiconductors," Phys. Rev B. Vol, 27, pp. 3494–3505, 1983.

[19] M. Tinkham, *Introduction to Superconductivity*, New York: McGraw-Hill, 1996.

[20] A. Yamamoto, N. Takeshita, C. Terakura, and Y. Tokura, "High pressure effects revisited for the cuprate superconductor family with highest critical temperature," Nat. Commun. Vol. 6, pp. 8990 (1-7), 2015.

[21] N. Takeshita, A. Yamamoto, A. Iyo, and H. Eisaki, "Zero resistivity above 150 K in $HgBa_2Ca_2Cu_3O_{8+\delta}$ at high pressure," J. Phys. Soc. Jpn. Vol. 82, pp. 023711 (1-4), 2013.

[22] G. Samara, "Temperature and pressure dependences of the dielectric constants of semiconductors," Phys. Rev. B, Vol. 27, pp. 3494-3505, 1983.

[23] A. Elabsy, "Hydrostatic pressure dependence of binding energies for donors in quantum well heterostructures," Phys. Scr. Vol. 48, pp. 376-378, 1993.

Samad Roshan Entezar received his B.S. degree (1996) in applied physics, his M.Sc.

degree (2001), and Ph.D. degree (2006) in laser physics from the University of Tabriz, Tabriz, Iran. He is currently a professor at the University of Tabriz, Tabriz, Iran, Department of Physics since 2008. His main research interests focus on the quantum optics, optical properties of photonic crystals, metamaterials, and nonlinear materials.